Earth and Planetary Science Letters 381 (2013) 52–62

Contents lists available at ScienceDirect

Earth and Planetary Science Letters

www.elsevier.com/locate/epsl

Deep Pacific ventilation ages during the last deglaciation: Evaluating the influence of diffusive mixing and source region reservoir age

David C. Lund *

Department of Earth and Environmental Sciences, University of Michigan, United States

ARTICLE INFO

Article history:
Received 29 August 2012
Received in revised form 24 July 2013
Accepted 6 August 2013
Available online xxxx
Editor: J. Lynch-Stieglitz

Keywords:
ventilation
deep Pacific
deglaciation
carbon cycle

ABSTRACT

Enhanced ventilation of the deep ocean during the last deglaciation may have caused the rise in atmospheric carbon dioxide that drove Earth's climate from a glacial to interglacial state. Recent results based on the projection age method, however, suggest the ventilation rate of the deep Pacific slowed during the deglaciation, opposite the expected pattern (Lund et al., 2011). Because the projection age method does not account for tracer diffusion (Adkins and Boyle, 1997) it can yield spurious results and therefore requires validation with alternative techniques. Here ventilation ages are determined using the transit-time equilibration-time distribution (TTD–ETD) method which explicitly accounts for diffusive mixing in the ocean interior (DeVries and Primeau, 2010). The overall time history of deep Pacific TTD–ETD and projection ages is very similar; both show a 1000-yr increase in ventilation age during Heinrich Stadial 1 (HS1; 14.5–17.5 kyr BP) and a 500-yr increase during the Younger Dryas (YD). The similarity is due in part to the use of projection age error estimates that take into account uncertainty in both calendar age and benthic ^{14}C age. Centennial-scale offsets between the TTD–ETD and projection ages are due primarily to the different approaches used to estimate surface ocean radiocarbon content. Both the TTD–ETD and projection age results imply that the ventilation rate of the deep Pacific decreased during the deglaciation, opposite the pattern expected if Southern Ocean upwelling and enhanced meridional overturning drove outgassing of CO_2 from the abyss. Variations in surface water reservoir age could cause an apparent shift in deep Pacific ventilation age but existing proxy records from the Southern Ocean appear to be inconsistent with such a driver.

1. Introduction

The transition from the Last Glacial Maximum (LGM; ~20 kyr BP) to the early Holocene (~10 kyr BP) is characterized by the disappearance of large continental ice sheets in North America and Eurasia (Clark et al., 2009), an apparent reorganization of the oceanic circulation (Curry and Oppo, 2005; Lynch-Stieglitz et al., 2007; Herguera et al., 2010; Hoffman and Lund, 2012), increasing atmospheric carbon dioxide levels (Monnin et al., 2001), and a rise in global average temperatures (Shakun et al., 2012). The reduction in planetary albedo due to melting of continental ice and the enhanced greenhouse effect due to elevated CO_2 levels are thought to be the primary amplifiers that forced the Earth's climate system from a glacial to interglacial state (Shakun et al., 2012).

Given the central role of atmospheric CO_2 in glacial–interglacial cycles, unraveling the processes that regulate CO_2 is one of the central goals of paleoclimate research. Because greater than 90% of oceanic, terrestrial, and atmospheric carbon resides in the deep ocean, the degree of carbon exchange between the deep ocean and atmosphere is thought to play a primary role in glacial–interglacial CO_2 variability (Sigman and Boyle, 2000). Release of carbon from the deep sea occurs primarily in the Southern Ocean where carbon-rich waters upwell to the surface (Lovenduski et al., 2007; Marshall and Speer, 2012). Reduced outgassing of CO_2 from the Southern Ocean may have caused lower atmospheric CO_2 levels during the LGM (Sigman et al., 2010) while enhanced upwelling and outgassing may have been the primary driver of rising atmospheric CO_2 during the last deglaciation (Anderson et al., 2009).

An increase in the ventilation rate of the deep ocean during the last deglaciation would cause its ventilation age (i.e., the time elapsed since water was last in contact with the atmosphere) to decrease. Because the deep Pacific represents ~50% of global ocean carbon inventory, constraining the ventilation age of this reservoir is key to understanding ocean–atmosphere carbon exchange. Using a 3-D carbon cycle model, Tschumi et al. (2011) found that an 80% increase in Southern Ocean wind stress causes atmospheric CO_2 to rise about 20 ppmv and the $\delta^{13}C$ of atmospheric CO_2 to decrease by ~0.2‰, similar to the changes observed early in the deglaciation (Monnin et al., 2001; Schmitt et al., 2012). The simulated global average deep water age below 2000 m decreased 250 yr,

* Current address: Department of Marine Sciences, University of Connecticut, Avery Point, United States.
E-mail address: david.lund@uconn.edu.

0012-821X/$ – see front matter
http://dx.doi.org/10.1016/j.epsl.2013.08.032

Table 1

Deep water source	Fraction[1]	Mean surface water reservoir age (yr)[2]	1σ	SE	n
Southern Ocean, <60°S	0.47	1130	190	48	16
Southern Ocean, 45°S–60°S	0.19	720	30	–	–
North Atlantic, 50°N–70°N	0.28	400	100	8	148
Surface Pacific, 40°S–40°N	0.04	430	180	8	415
North Pacific, >40°N	0.02	690	150	18	70

[1] Fraction for the deep Northeast Pacific (42°N, 126°W, 2700 m) from Gebbie and Huybers (2012).
[2] Calculated using data from the CALIB Marine Reservoir Database (http://calib.qub.ac.uk/marine/). Due to a lack of data in the sub-Antarctic, the reservoir age estimate for 45°S–60°S is based on the surface water ^{14}C age for this region in Gebbie and Huybers (2012) (860 ± 30 yr) minus the average atmospheric ^{14}C age for all of the data in the CALIB database (140 ± 10 yr) (Reservoir Age = Marine ^{14}C Age – Atmospheric ^{14}C Age).

with a reduction of about 100 yr in the deep Pacific. In contrast, a compilation of projection ages from the deep Pacific suggests the ventilation age increased by more than 500 yr during the deglaciation (Lund et al. 2011). Thus, there appears to be a fundamental disagreement between model predictions of ventilation age and observational constraints from the paleoceanographic record.

The primary aim of this paper is to evaluate whether confounding factors associated the projection age method may yield spurious ventilation ages. Projection ages do not explicitly account for either (1) mixing in the ocean interior, or (2) changes in source region reservoir age. To address the first point, ventilation ages are determined using the transit-time distribution, equilibration-time distribution (TTD–ETD) method developed by DeVries and Primeau (2010) (hereafter DP10). The second point is evaluated by inverting deep Pacific $\Delta^{14}C$ to determine the changes in Southern Ocean reservoir age required to produce the deep $\Delta^{14}C$ data and then comparing the resulting time series to published records from the Southern Ocean.

2. Methods

2.1. Revised projection ages

The projection age method developed by Adkins and Boyle (1997) marked an important advancement in the study of the paleo-ventilation ages because it was the first to explicitly account for the history of atmospheric $\Delta^{14}C$. Prior to the projection age method, the most common approach for determining ventilation ages involved subtracting the planktonic foraminiferal ^{14}C age from the benthic foraminiferal ^{14}C age in the same sample (a.k.a. benthic–planktonic or B–P age). Although the method is appealing in its simplicity, Adkins and Boyle (1997) clearly demonstrated that B–P ages yield biased results if atmospheric $\Delta^{14}C$ varies through time. Given that most of the last 50,000 yr is characterized by substantial variations in atmospheric $\Delta^{14}C$ (Reimer et al., 2009), B-P ages are generally unreliable for estimating ventilation age.

The original projection age method takes the atmospheric radiocarbon history into account by projecting a given deep ocean $\Delta^{14}C$ estimate along its decay trajectory until it intersects the atmospheric $\Delta^{14}C$ curve (Adkins and Boyle, 1997). The difference in calendar age of the $\Delta^{14}C$ estimate and the intersection point with the atmospheric $\Delta^{14}C$ curve is known as the projection age relative to the atmosphere. To obtain a true ventilation age (that is, one that reflects the time elapsed since water was last in contact with the atmosphere), the surface water reservoir age in the deep water formation region is subtracted from the projection age relative to the atmosphere.

Lund et al. (2011) used the projection age method to create a high resolution record of ventilation ages for the deep Northeast Pacific from 20 to 8 kyr BP. Each benthic $\Delta^{14}C$ estimate was projected back to the atmospheric $\Delta^{14}C$ curve. Because the Southern Ocean is the primary source of deep water in the Pacific (Gebbie and Huybers, 2010), the surface water reservoir age for the Southern Ocean was then subtracted to determine the projection age. Lund et al. (2011) used a surface water reservoir age of 1100 ± 200 yr (1σ) estimated using the data from south of 60°S in the CALIB Marine Database (http://calib.qub.ac.uk/marine/).

Here a revised projection age method is used that projects benthic $\Delta^{14}C$ values back to a surface ocean $\Delta^{14}C$ curve because it better represents the actual decay trajectory a given water parcel would take as it moves from the surface ocean into the abyss. As in Lund et al. (2011), errors in calendar age and benthic ^{14}C age are fully propagated using a Monte Carlo approach to create 1000 estimates of $\Delta^{14}C$ for each benthic sample.

Each of the $\Delta^{14}C$ estimates is then projected back to the surface ocean $\Delta^{14}C$ curve to create a distribution of possible projection ages. This approach prevents spurious projection age estimates that can result from abrupt peaks in the surface ocean $\Delta^{14}C$ history. The revised method was followed to determine projection ages for published data from the Northeast Pacific (Galbraith et al., 2007; Gebhardt et al., 2008; Lund et al. 2011) and the western equatorial Pacific (Broecker et al., 2008).

The surface ocean $\Delta^{14}C$ curve was constructed assuming a constant surface water reservoir age for waters that enter the deep Pacific. Unlike in Lund et al. (2011), a weighted approach was used to take into account the proportion of water at 2700 m in the North Pacific originating from different locations (Table 1). Each proportion was multiplied by its corresponding mean surface water reservoir age and the resulting values were summed to yield a net reservoir age of 810 ± 460 yr (1σ). Using the standard errors in Table 1, which reflect uncertainty in the mean reservoir age for each region, the propagated uncertainty for the net reservoir age is ± 70 yr. An 810-yr reservoir age better represents the 'preformed' age of the source waters for the deep Pacific than the 1100-yr value used in Lund et al. (2011) and is consistent with estimates of 800–900 yr based on modern observations (Gebbie and Huybers, 2012; Khatiwala et al., 2012). Increasing (decreasing) the reservoir age shifts the projection ages to lower (higher) values but has little influence on the relative change through time.

2.2. TTD–ETD ages

One of the shortcomings of the projection age method is that it does not account for mixing in the ocean interior. In reality, the radiocarbon content of a water parcel in the deep ocean reflects both radiocarbon decay from its point of origin but also mixing with other water parcels that are both older and younger. In this sense, the radiocarbon age of the deep Pacific represents a range of advective pathways from the surface ocean into the abyss. To account for this more complex picture, DP10 argued that paleo-ventilation ages should instead be determined using the TTD method.

The TTD approach is based on the premise that the range of transit times from the surface ocean into the ocean interior can be parameterized and used to capture the effects of advection and diffusion on ^{14}C ages. Similar to the projection age approach, it assumes that most of the water in the deep Pacific originates from

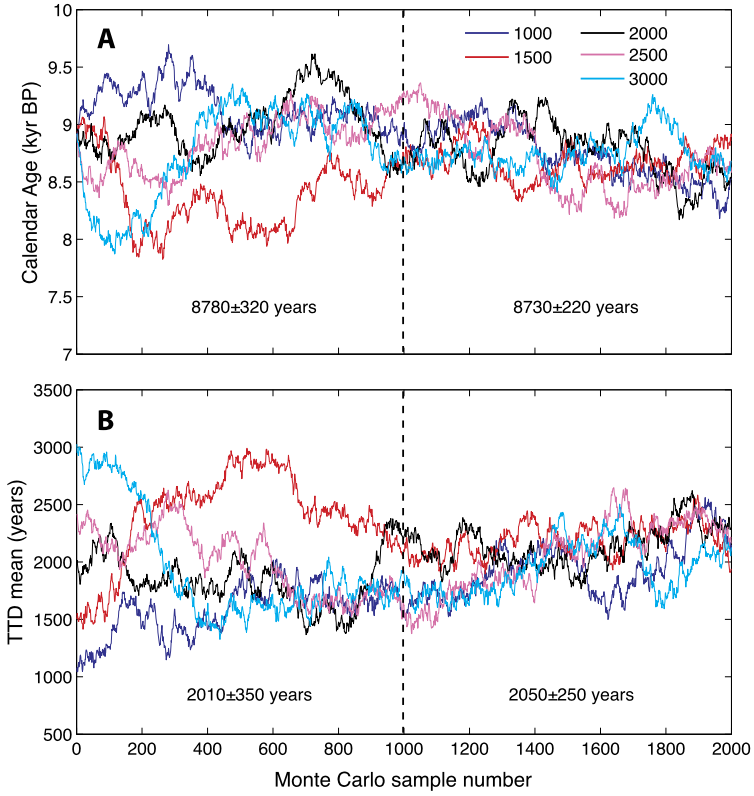

Fig. 1. (A) Calendar age vs. Monte Carlo sample number for the benthic–planktonic radiocarbon pair at 8.8 kyr BP. Each curve represents the sampling evolution over 2000 iterations based on an initial TTD mean of 1000 yr (dark blue), 1500 yr (red), 2000 yr (black), 2500 yr (magenta), and 3000 yr (light blue). The Monte Carlo chains converged on a common value after 1000 iterations, typical of samples for W8709A-13PC and MD01-2386. We used the final 1000 iterations of each chain to calculate the mean calendar age (8730 ± 230 yr) (1σ). The mean is similar if the first 1000 iterations are used (8780 yr) but the standard deviation is greater (320 yr). (B) TTD mean vs. Monte Carlo sample number for the benthic–planktonic pair at 8.8 kyr BP. Lines are the same as in (A). The final 1000 iterations of each chain were used to calculate the mean TTD (2050 ± 250 yr) (1σ). The mean is similar if the first 1000 iterations are used (2010 yr) but the standard deviation is greater (350 yr). Higher mean TTD estimates in each chain correspond to younger calendar ages. (For interpretation of the references to color in this figure legend, the reader is referred to the web version of this article.)

a single source region. An inversion of modern tracer data suggests about 70% of the water in the deep North Pacific originates in the Southern Ocean (Gebbie and Huybers, 2010) (Table 1). The method does not account for other watermasses or sources of carbon that may have influenced the deep Pacific during the LGM and deglaciation.

The method presented by DP10 uses an equilibration time distribution (ETD) to account for the range of equilibration times with the atmosphere due to the slower air–sea exchange rate of $^{14}CO_2$ relative to $^{12}CO_2$. The ETD constrains the preformed $\Delta^{14}C$ of deep waters while the TTD constrains the distribution of transit times (i.e. ventilation ages) from the surface Southern Ocean to any given point in the deep Pacific. A primary benefit of the ETD is that it captures the lagged response time of the surface ocean to changing atmospheric $\Delta^{14}C$. This memory effect can yield changes in surface water reservoir age on the order of hundreds of years (Franke et al., 2008).

Following the ocean general circulation model results presented in DP10, the prior probability density function (pdf) for the ETD was parameterized using a mean (Θ_e) of 900 yr and scale parameter (β_e) of 1600 yr. The scale parameter represents the ratio of ETD variance to the mean. Unlike the TTD, which has an approximately normal distribution, the ETD is a lognormal distribution designed to capture both the relatively rapid equilibration of surface waters and the slow exchange with the more poorly ventilated parts of the deep ocean. The prior pdf for the TTD was parameterized using a scale parameter (β_v) of 600 yr. Note that for the remainder of the paper the term width is used interchangeably with scale parameter to describe the variance of the TTD and ETD.

For each benthic ^{14}C age from core W8709A-13PC, a joint posterior pdf of calendar ages and TTD ages was generated using the Matlab code provided by Tim DeVries. The routine uses a Monte Carlo approach to sample the prior TTD and ETD distributions and estimate a benthic ^{14}C age based on the calendar age of the sample and the atmospheric ^{14}C history. INTCAL09 was used as the atmospheric $\Delta^{14}C$ history because it is the basis of the calendar ages outlined in Lund et al. (2011). The estimated benthic ^{14}C age is compared to the actual benthic ^{14}C age for a given sample using a likelihood function (Eq. 9 in DP10) and the mean TTD (Θ_v) is then varied iteratively to improve the fit between the estimated and actual benthic ^{14}C age.

Five separate Monte Carlo Markov chains of 2000 samples each were used to evaluate the TTD mean. To ensure the results were insensitive to the choice of the initial values, initial mean TTDs of 1000, 1500, 2000, 2500, and 3000 yr were used. This range spans the full spectrum of projection age results in Lund et al. (2011). Each chain typically converged on a common value after 1000 samples, so the last 50% of each chain was used to determine the mean transit time associated with each benthic ^{14}C age (Fig. 1). If all of the data from each chain are used the mean transit time changes only slightly and the variance increases. Higher mean TTD values in Fig. 1 correspond to younger calendar ages because a longer transit time is necessary to reconcile the benthic ^{14}C age and atmospheric $\Delta^{14}C$ history.

Fig. 2 shows the TTD and ETD parameters associated with the benthic–planktonic pair at 8.8 kyr BP. The top row includes histograms of the TTD mean, TTD width, ETD mean, and ETD width. The mean TTD for this benthic–planktonic pair is 2050 ± 250 yr while the mean ETD is 790 ± 210 yr. The mean ETD is analo-

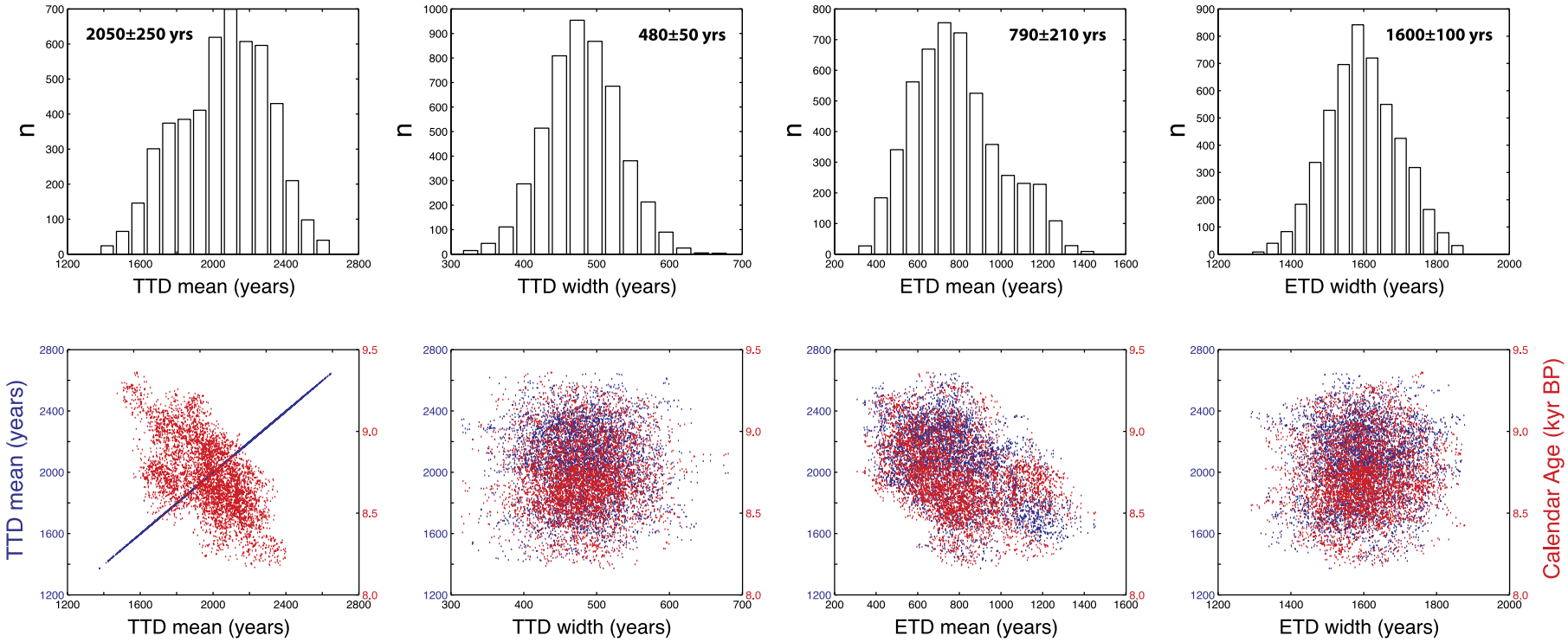

Fig. 2. (Top row) Histograms of the TTD mean, TTD width, ETD mean, and ETD width for the benthic–planktonic radiocarbon pair at 8.8 kyr BP. Values in bold are the means and 1σ uncertainties for each parameter. The histograms show the last 1000 samples from each Monte Carlo chain (total $n = 5000$). (Bottom row) Plot of each parameter in the first row vs. TTD mean (blue dots) and calendar age (red dots). The strong negative correlation between TTD mean and calendar age in the first panel is a result of younger calendar ages requiring longer transit times for a given benthic ^{14}C age and atmospheric radiocarbon history. Higher ETD means also correspond to shorter transit times, but the correlation is weaker (third panel). The TTD width (second panel) and ETD width (fourth panel) show no correlation with either the TTD mean or calendar age. (For interpretation of the references to color in this figure legend, the reader is referred to the web version of this article.)

gous to the surface reservoir age of source waters for the Pacific and is similar to the net surface water reservoir age of 810 yr used to constrain the surface ocean $\Delta^{14}C$ history for the projection age estimates. The bottom row of Fig. 2 shows cross plots of the parameters in the first row versus the TTD mean (blue points) and calendar age (red points). As expected, there is strong negative correlation between the mean TTD values and calendar age. The TTD mean is less sensitive to the choice of the ETD mean but still shows a negative correlation because higher ETD ages in the source region require shorter transit times. Neither the TTD mean nor calendar age correlate with the TTD width or the ETD width, indicating the results are insensitive to choice of scale parameter. As discussed in DP10, the scale parameters have little impact on the TTD ages so long as the values are sufficiently large (e.g. a TTD width >250 yr and an ETD width >900 yr).

3. Results and discussion

3.1. Deep Pacific $\Delta^{14}C$

Benthic $\Delta^{14}C$ results for the deep Pacific are shown in Fig. 3A, including data from 2.7 km water depth in the NE Pacific (Lund et al. 2011), 3.6 km in the subarctic NE Pacific (Galbraith et al., 2007; Gebhardt et al., 2008), and 2.8 km in the western equatorial Pacific (Broecker et al., 2008). Details of the calendar age control used for each core are given in Lund et al. (2011). Also shown in Fig. 3A are the INTCAL09 atmospheric $\Delta^{14}C$ curve and the estimated surface ocean $\Delta^{14}C$ assuming a surface water reservoir age of 810 yr (see Methods). The surface ocean time series is the curve to which benthic $\Delta^{14}C$ values were projected to determine the revised projection ages. The dashed black line in Fig. 3A represents the predicted $\Delta^{14}C$ for the deep Pacific from 0 to 25 kyr BP. It is based on the parameterized TTD from DP10 (Eq. 5) assuming a TTD mean (Θ) of 1500 yr and width (β) of 600 yr. The TTD mean is similar to that inferred from modern $\Delta^{14}C$ observations (~1400 yr; Gebbie and Huybers, 2012) and general circulation model results (~1600 yr; DeVries and Primeau, 2010).

Most of the benthic $\Delta^{14}C$ estimates for the past 25 kyr overlap with the predicted deep Pacific $\Delta^{14}C$ curve with the exception of data from approximately 10 to 12 kyr BP and 14 to 17 kyr BP. During these two intervals, the deep Pacific was radiocarbon deficient compared to today, either due to lower preformed $\Delta^{14}C$ in the deep water source region(s) or longer transit times from the surface ocean to the deep Pacific. These possibilities are discussed in detail in the following sections.

For the LGM (19–23 kyr BP), $\Delta^{14}C$ estimates for the deep Pacific are within error of one another and generally fall between 0‰ and 100‰. Given that individual $\Delta^{14}C$ values tend to overlap with the predicted $\Delta^{14}C$ curve, it appears that the circulation of the deep Pacific was similar to today. However, averaging data by water depth, the results from 2.7 km in the NE Pacific yield an average $\Delta^{14}C$ of 59 ± 12‰ ($\pm$1SE; $n = 6$) while the data at 3.6 km yield an average $\Delta^{14}C$ of 6 ± 5‰ ($\pm$1SE; $n = 6$). Although tentative given the limited number of data points, it appears that $\Delta^{14}C$ of the deep NE Pacific at 3.6 km was approximately 50‰ lower than at 2.7 km during the LGM.

In the modern NE Pacific, Lower Circumpolar Deep Water enters the NE Pacific Basin and is altered via geothermal heating and diapycnal mixing to form North Pacific Deep Water, which flows southward at depths above 4 km (Mantyla, 1975; Kawabe and Fujio, 2010). As a result, $\Delta^{14}C$ at 2.7 km water depth (-247 ± 4‰; 1σ) is approximately 20‰ lower than at 3.6 km (-226 ± 4‰; 1σ) (Key et al., 2004). If the LGM vertical gradient was opposite the modern gradient, it would imply that the circulation pattern in the NE Pacific was substantially different. Given that the available LGM $\delta^{13}C$ data do not show clear evidence for a reversed vertical $\delta^{13}C$ gradient in the NE Pacific (Herguera et al., 2010), the preliminary LGM $\Delta^{14}C$ results require verification with a more complete vertical transect of $\Delta^{14}C$ estimates.

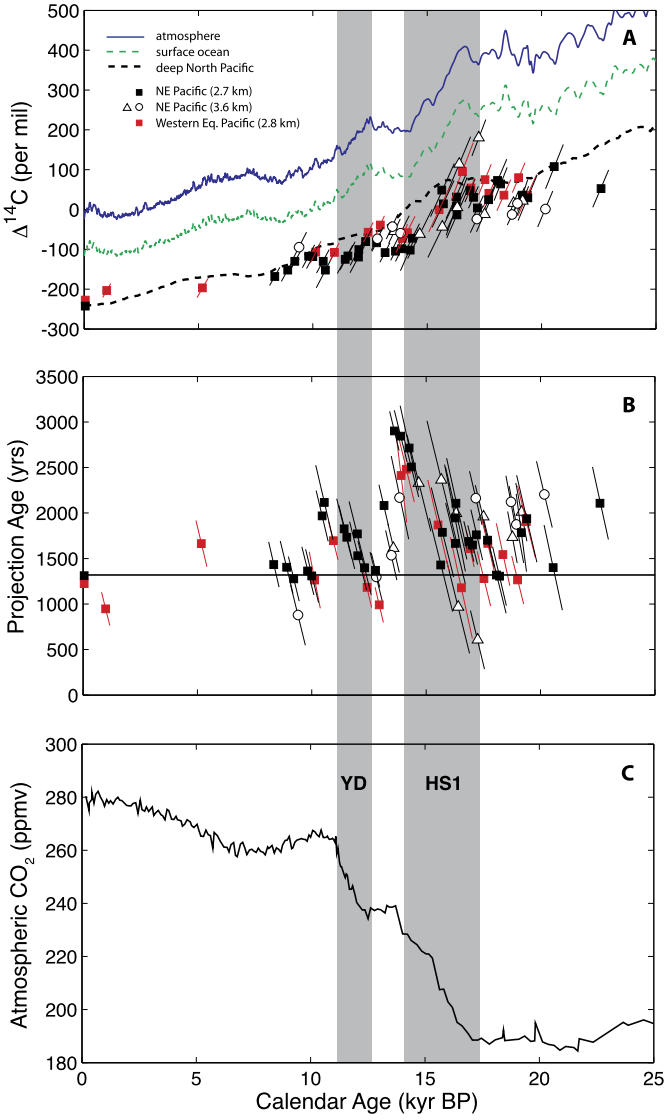

Fig. 3. (A) INTCAL09 atmospheric $\Delta^{14}C$ (blue), surface Southern Ocean $\Delta^{14}C$ assuming an 810-yr surface water reservoir age (green), and predicted deep Pacific $\Delta^{14}C$ (black line). Also shown are deep Pacific $\Delta^{14}C$ data from Lund et al. (2011) (black squares), Gebhardt et al. (2008) (white triangles), Galbraith et al. (2007) (white circles), and Broecker et al. (2008) (red squares). Results at 0 kyr BP are based on GLODAP data for the deep Pacific (Key et al., 2004). Predicted deep Pacific values were calculated using a TTD with mean 1500 yr and width of 600 yr. Benthic $\Delta^{14}C$ values lower than the predicted curve represent radiocarbon deficient intervals relative to modern. (B) Projection age estimates for all deep Pacific sites using symbols as defined in the top panel. Projection ages increased during Heinrich Stadial 1 (HS1) (17.5–14.5 kyr BP; McManus et al., 2004) and the Younger Dryas (YD) (12.9–11.7 kyr BP; Rasmussen et al., 2006) (grey vertical bars). The horizontal black line is the modern projection age (1350 yr) for the 2.7 km water depth in the NE Pacific. The modern projection age for 2.8 km water depth in the western equatorial Pacific is 1220 yr. (C) Atmospheric CO_2 from Taylor Dome, Antarctica (Monnin et al., 2004). Intervals of increasing CO_2 correspond to increasing deep Pacific projection ages. (For interpretation of the references to color in this figure legend, the reader is referred to the web version of this article.)

3.2. Revised projection ages

The largest changes in projection age occurred early in the deglaciation, with the results indicating a 1 kyr increase during HS1 (Fig. 3B). Projection ages at 2.7–2.8 km water depth also increased approximately 500 yr during the Younger Dryas (YD). The YD anomaly is now evident because the revised projection age

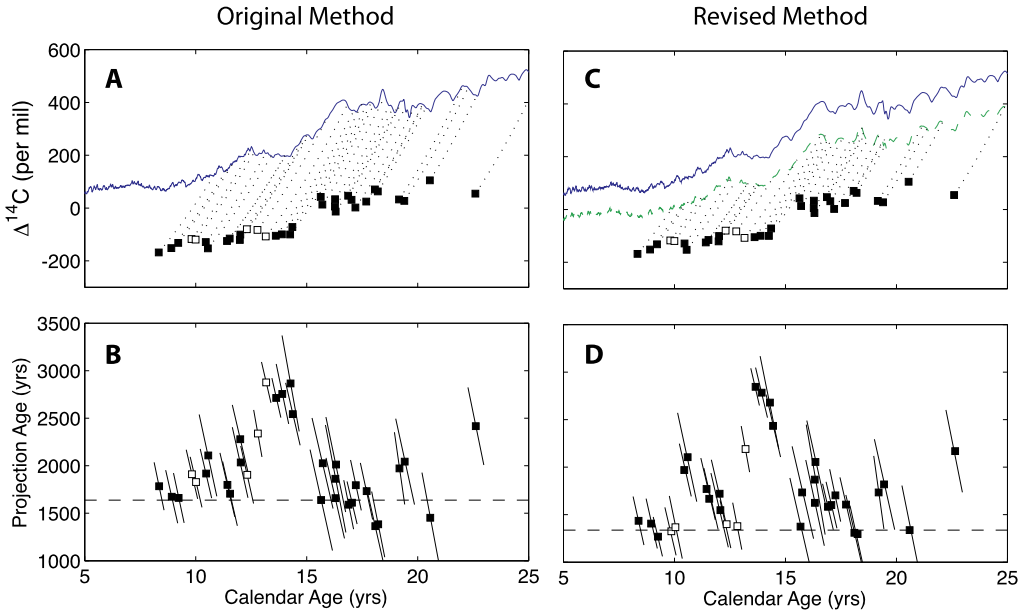

Fig. 4. (A) Projection trajectories (dotted lines) between W8709A-13PC benthic $\Delta^{14}C$ results (black squares) and the INTCAL09 atmospheric $\Delta^{14}C$ curve (solid line). The difference in calendar age between each benthic $\Delta^{14}C$ result and its intersection point with the atmosphere is the projection age relative to the atmosphere. (B) Projection ages determined by subtracting a surface water reservoir age of 810 yr from the projection age relative to the atmosphere. Points with significantly different projection ages based on the revised method are shown as white squares (see text for details). (C) Same as panel (A) but projection trajectories intersect a surface ocean $\Delta^{14}C$ curve rather than the atmospheric curve. (D) Revised projection ages estimated by determining the difference in calendar age between each benthic $\Delta^{14}C$ result and its intersection point with the surface ocean $\Delta^{14}C$ curve.

method projects benthic $\Delta^{14}C$ values back to the surface ocean rather than atmospheric $\Delta^{14}C$ curve (Fig. 4). For example, benthic $\Delta^{14}C$ results at ~10 kyr BP (white squares) intersect an interval of high atmospheric $\Delta^{14}C$ (Fig. 4A) but relatively low surface ocean $\Delta^{14}C$ (Fig. 4C). A similar phenomena occurs for benthic $\Delta^{14}C$ results at ~13 kyr BP. In each case, the revised method makes the projection ages younger because the intersection points occur after a major decrease in $\Delta^{14}C$ rather than before. The net effect is a time series where projection age maxima during HS1 and the YD are more pronounced because of younger projection ages at the end of each interval (Fig. 4D).

Given the lack of data at 3.6 km water depth during the YD it is unclear whether projection ages also increased deeper in the water column. However, it does appear that ages at 3.6 km water depth increased during HS1 and then decreased rapidly from 14 to 13 kyr BP (Fig. 3B). The decrease is broadly consistent with circumstantial evidence for increased ventilation rate below 3 km water depth in the subarctic North Pacific, including lower sedimentary uranium concentrations, higher $\%CaCO_3$, and higher benthic $\delta^{13}C$ (Galbraith et al., 2007; Gebhardt et al., 2008). These proxies lack a clear signal during HS1 and the YD, however, suggesting they are relatively insensitive to decreases in ventilation rate during the deglaciation. In the case of $\%CaCO_3$, such a result would not be surprising given that it was at or near 0% during the LGM (Galbraith et al., 2007).

3.3. TTD results

The results of the TTD–ETD analysis for the NE Pacific (W8709A-13PC) and western equatorial Pacific (MD01-2386) are shown in Fig. 5B. Projection ages are shown in Fig. 5A for comparison. The overall ventilation age histories are very similar. Both the projection and TTD ages suggest the mean LGM ventilation age of the Pacific at 2.7–2.8 km water depth was indistinguishable from today. During the deglaciation, TTD and projection ages increased by approximately 1 kyr during HS1, declined ~1 kyr after HS1, and increased ~500 yr during the YD. After the YD, both methods show a return to ventilation ages within error of the modern.

Given that DP10 emphasized the differences in projection ages and TTD ages, the results in Fig. 5 are somewhat surprising. However, DP10 found that the difference between projection and TTD ages were typically 200 yr or less (see their Fig. 4). Here we find a similar pattern using paleo-data from the Northeast Pacific and western equatorial Pacific. The mean offset is 170 ± 230 yr (1σ) (Fig. 5C). Given that variations in ventilation age during the deglaciation are larger than the typical offset between TTD and projection ages, the discrepancy between the methods is less obvious than in an idealized scenario. Also, the uncertainty in projection ages is determined here by fully propagating the error in both benthic ^{14}C ages and the planktonic calendar ages. Anomalous projection ages that occur from projecting benthic $\Delta^{14}C$ values to high frequency variations in the surface ocean $\Delta^{14}C$ curve are therefore minimized.

The largest contrast between the methods occurs near 13 kyr BP, where the projections ages are all very close to the modern value, whereas the TTD ages are somewhat higher than their modern counterpart. Also, the clear increase in projection ages during the Younger Dryas is less apparent in the TTD results due to the greater variability in TTD ages from 10 to 12 kyr BP. There are also individual cases where the mean projection age is clearly offset from the mean TTD age. For example, the projection age at 9 kyr BP is 1400 yr compared to a TTD age of 2000 yr.

Offsets between the projection and TTD ages are primarily driven by the different approaches used to estimate surface water reservoir age. The projection ages are based on a surface ocean $\Delta^{14}C$ curve estimated using an 810-yr reservoir age. The TTD method, on the other hand, relies on a surface ocean $\Delta^{14}C$ curve constructed using an equilibration time distribution (ETD). The ETD is designed to mimic the full range surface ocean ^{14}C equilibration times observed in ocean general circulation models, from very short (5–10 yr) to very long (thousands of years) (DeVries and Primeau, 2010). Because the tail of the ETD extends thousands of years into the past, surface ocean $\Delta^{14}C$ values calculated using an ETD will have a memory of atmospheric $\Delta^{14}C$ from the preceding millennia. Given that atmospheric $\Delta^{14}C$ decreased over the past

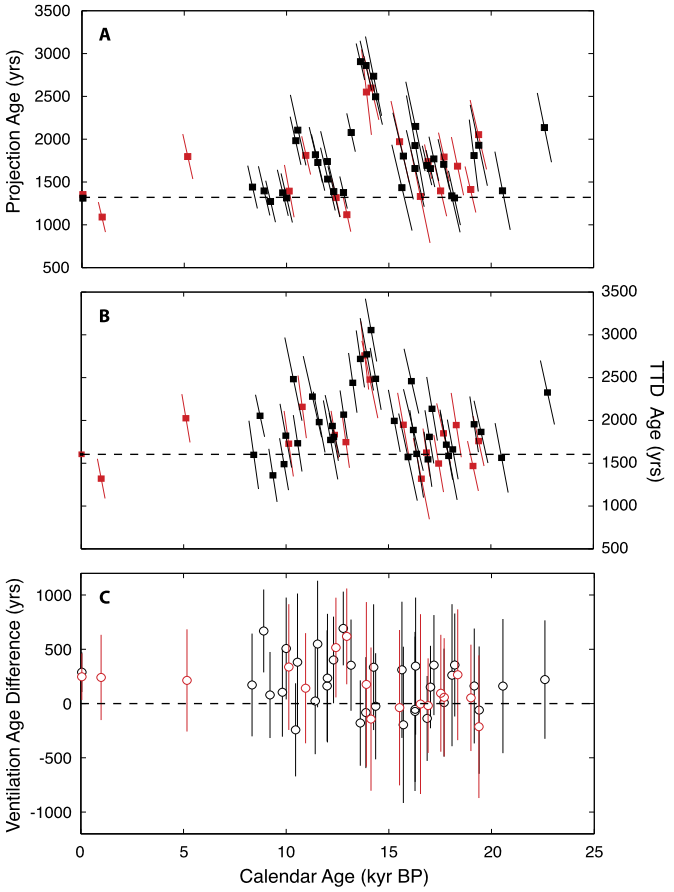

Fig. 5. (A) Time series of projection ages for the NE Pacific (W8709A-13PC; black squares) and western equatorial Pacific (MD01-2386; red squares). Error bars represent $\pm 1\sigma$ uncertainties. For MD01-2386, 130 yr has been added to each projection age (the difference in modern projection age between the two sites) to facilitate comparison with W8709A-13PC. Also shown is the modern projection age for the NE Pacific (1350 yr; dashed line). (B) Time series of mean TTD ages for W8709A-13PC (black squares) and MD01-2386 (red squares) based on the TTD–ETD method of DeVries and Primeau (2010). Error bars represent $\pm 1\sigma$ uncertainties. For MD01-2386, 180 yr has been added to each TTD age (the difference in modern TTD age between the two sites) to facilitate comparison to W8709A-13PC. The modern TTD age for the NE Pacific (dashed horizontal line) is also shown (1600 yr). (C) The difference between mean TTD age and mean projection age (circles), including the $\pm 1\sigma$ uncertainty (vertical lines). In most cases, the differences are within 1σ of zero years but in isolated cases the offset between TTD and projection ages can reach several hundred years (e.g. at ~13 kyr BP). On average, the TTD ages are 170 ± 230 yr (1σ) older than the projection ages. (For interpretation of the references to color in this figure legend, the reader is referred to the web version of this article.)

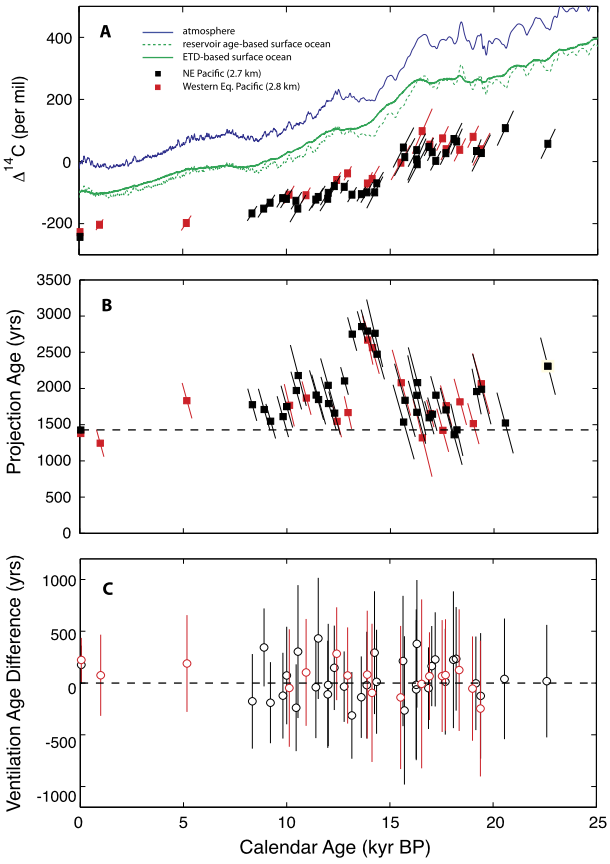

Fig. 6. (A) INTCAL09 atmospheric $\Delta^{14}C$ (blue), surface ocean $\Delta^{14}C$ assuming an 810-yr surface water reservoir age (dashed green), and surface ocean $\Delta^{14}C$ based on an ETD with mean of 900 yr and scale parameter of 1600 yr (solid green). Also shown are the reconstructed $\Delta^{14}C$ values for the deep NE Pacific (black squares) (Lund et al. 2011) and the western equatorial Pacific (red squares) (Broecker et al., 2008). (B) Projection ages determined by un-decaying each benthic $\Delta^{14}C$ estimate until it intersects the ETD-based surface ocean $\Delta^{14}C$ curve. (C) The difference between the mean TTD age in Fig. 5B and mean projection age in Fig. 6B (vertical lines are the $\pm 1\sigma$ uncertainty). In all cases the difference is within 1σ of zero years. The average difference between the methods is 40 ± 170 yr (1σ). Note that the 500-yr offset in Fig. 5C near 13 kyr BP has disappeared. (For interpretation of the references to color in this figure legend, the reader is referred to the web version of this article.)

25,000 yr, the ETD-based surface ocean $\Delta^{14}C$ curve will generally be younger than that based on a constant reservoir age (Fig. 6A). The difference between the two curves is typically 20‰ but at times when atmospheric $\Delta^{14}C$ drops quickly (e.g. 17 to 14 kyr BP) the offset is up to 50‰. If benthic $\Delta^{14}C$ estimates are projected back to the ETD-based curve the resulting projection ages (Fig. 6B) are very similar to those based on the TTD–ETD method. The difference between the two time series is negligible, with an average offset of 40 ± 170 yr (Fig. 6C). Thus, the primary difference between projection ages and TTD–ETD ages is due to the ETD rather than the TTD.

The finding of similar TTD and projection age results in the paleo-record is consistent with studies that address the effect of diffusive mixing on $\Delta^{14}C$ in the modern ocean. Both Gebbie and Huybers (2012) and Khatiwala et al. (2012) found that neglecting TTD width biases ventilation ages by less than 100 yr. Here we find that the ignoring the TTD width by using the projection age method and an ETD-based surface ocean $\Delta^{14}C$ curve yields biases of a similar magnitude.

The TTD–ETD approach is superior to projection ages from a theoretical standpoint because it accounts for a range of ventilation ages and equilibration times but practically speaking the difference between the methods is small in the context of paleoceanographic uncertainties. The uncertainty associated with each projection age (on the order of ±300 yr) is a combination of analytical uncertainty, calendar calibration, geological imperfections (e.g. bioturbation), and errors due to projecting onto a surface ocean $\Delta^{14}C$ curve. The large (>500 yr) ventilation age signal during the last deglaciation also makes centennial-scale differences between the two methods less critical. In cases where the expected ventilation age signal is comparable to the typical offset between projection and TTD ages (~200 yr), the TTD–ETD method is clearly preferable. Unfortunately the noise inherent to benthic foraminiferal $\Delta^{14}C$ estimates may preclude reliable estimates of ventilation age in this scenario.

3.4. Changes in source region reservoir age

Given that explicitly accounting for mixing has a relatively minor impact on the overall deglacial ventilation age history in the

Pacific, we are left to consider whether changes in source region reservoir age may have driven the apparent anomalies in deep ocean ventilation. Neither the projection age nor the TTD–ETD method accounts for the possibility of large changes in this parameter.

Assuming that ventilation ages remained constant through time, the required change in surface water reservoir age to create the observed deep NE Pacific $\Delta^{14}C$ history can be estimated by 'un-decaying' each benthic $\Delta^{14}C$ data point in the NE Pacific by the modern projection age of 1350 yr. Similarly, each benthic $\Delta^{14}C$ result from Broecker et al. (2008) can be corrected for the modern projection age in the western equatorial Pacific of 1250 yr. The resulting time series, depicted as open squares in Fig. 7A, represent the surface ocean $\Delta^{14}C$ history necessary to account for the deep Pacific projection age anomalies during HS1 and the YD. The difference between these values and the surface ocean $\Delta^{14}C$ history represents the required change in surface ocean $\Delta^{14}C$ ($\Delta\Delta^{14}C$).

Estimates of $\Delta\Delta^{14}C$ were made using a surface ocean $\Delta^{14}C$ curve based on a constant 810-yr reservoir age (Fig. 7B) and an ETD with mean 900 yr and scale parameter of 1600 yr (Fig. 7C). Each approach suggests that two intervals of older surface water are required. The first spans the time range from approximately 18 kyr BP to 14.5 kyr BP. Given the scatter in the data, the initial increase in age may have occurred anywhere between 19 kyr BP and 17 kyr BP. The timing of the second $\Delta\Delta^{14}C$ anomaly is better constrained, occurring from approximately 13.0 kyr BP to 11.5 kyr BP. In each case, the magnitude of the signal is substantial. The first $\Delta\Delta^{14}C$ anomaly is 100–120‰, equivalent to a increase in surface water reservoir age of 800–1000 yr. The second is closer to 60‰ or about 500 yr. The primary difference in the two $\Delta\Delta^{14}C$ reconstructions is that the ETD-based estimates are more coherent between 19 and 17 kyr BP and the maximum anomaly at 15 kyr BP is 20–30‰ larger than that inferred using the reservoir age approach.

Reconstructions of surface water reservoir age histories in the Southern Ocean are exceedingly rare. The one estimate in the published literature is from 44°S in the Atlantic sector of the Southern Ocean, approximately 10° north of the Antarctic Polar Front (Skinner et al., 2010). The record implies that surface water reservoir age was higher than today from approximately 24 to 15 kyr BP and 14 to 13 kyr BP (Fig. 7C; dashed line). The $\Delta\Delta^{14}C$ and reservoir age reconstructions are clearly very different. Reservoir ages in the Skinner et al. (2010) reconstruction peak at 19 kyr BP, return to background values by 15 kyr BP and peak again at 13.5 kyr BP. The $\Delta\Delta^{14}C$ record shows nearly the opposite pattern; it peaks at 16 kyr BP, returns to background values by 14 kyr BP, and peaks again at 12–13 kyr BP. Although errors in the reservoir age estimates are substantial (±500 yr; Skinner et al., 2010), they do not appear to be large enough to allow for agreement with the $\Delta\Delta^{14}C$ record. Thus, the one existing record from the Southern Ocean does not support the idea that changes in surface water reservoir age drove the deep Pacific ventilation age history during the last deglaciation.

The preceding discussion is based on the premise that reservoir ages at 44°S in the Atlantic sector of the Southern Ocean are representative of the surface waters that feed into the deep Pacific. However, nearly half of the water in the deep Northeast Pacific originates south of the Antarctic Polar Front (Table 1). While there are no published time series of surface water reservoir age in this region, records of opal flux do exist (Anderson et al., 2009). To the extent that opal preservation in underlying sediments represents upwelling of ^{14}C-depleted water, time series of opal flux can be used as a qualitative proxy for surface water reservoir age.

The Southern Ocean opal flux records from Anderson et al. (2009) are shown in Fig. 7D. Opal flux increased abruptly at 16.0±0.5 kyr BP and remained high until ~10 kyr BP, with a brief return to lower values between 13 and 14 kyr BP. The $\Delta\Delta^{14}C$ estimates imply there was an initial increase in surface water reservoir age between 20 and 17 kyr BP, an interval of low values from 13 and 14 kyr BP, followed by a brief increase during the Younger Dryas. Given the age uncertainty in both records, the opal flux and

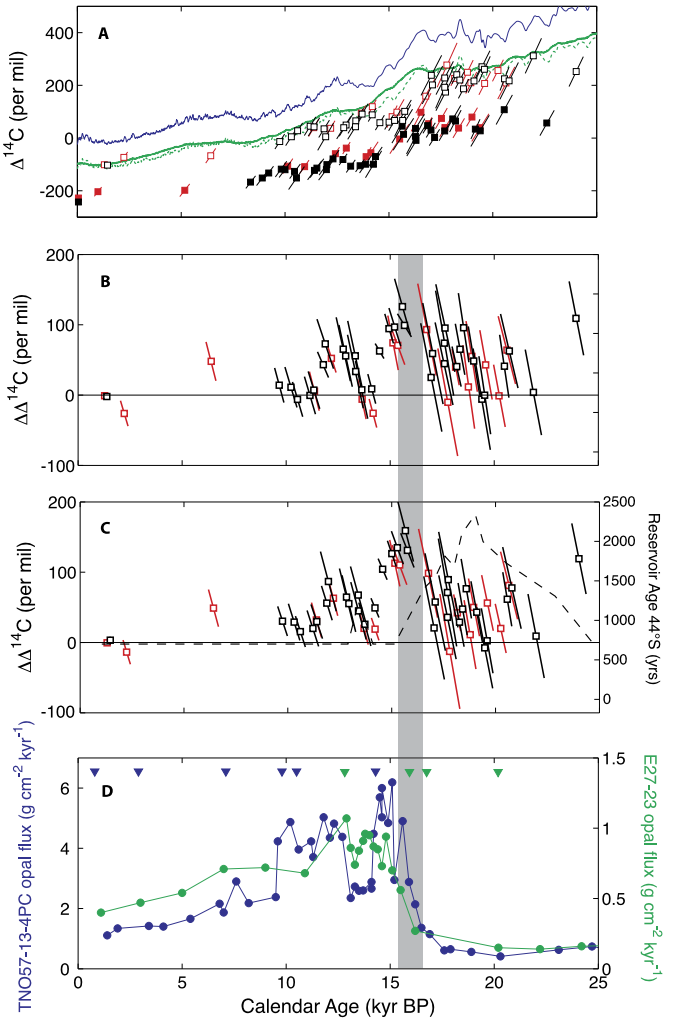

Fig. 7. (A) INTCAL09 atmospheric $\Delta^{14}C$ (blue), surface ocean $\Delta^{14}C$ assuming an 810-yr surface water reservoir age (dashed green), and surface ocean $\Delta^{14}C$ based on an ETD with mean of 900 yr and scale parameter of 1600 yr (solid green line). Also shown are reconstructed $\Delta^{14}C$ values from the NE Pacific (solid black squares) (Lund et al. 2011) and estimates of surface ocean $\Delta^{14}C$ assuming a constant 1350-yr projection age (open black squares). Benthic $\Delta^{14}C$ values for the western equatorial Pacific (Broecker et al., 2008) are shown as solid red squares while the corresponding estimates of surface ocean $\Delta^{14}C$ (assuming a constant 1220-yr projection age) are shown as open red squares. (B) Estimates of the change in surface ocean $\Delta^{14}C$ ($\Delta\Delta^{14}C$) required to account for the observed projection ages for the deep NE Pacific (open black squares) and western equatorial Pacific (open red squares). The reference surface ocean $\Delta^{14}C$ curve is based on an assumed 810-yr reservoir age (dashed green line in panel A). Two intervals of older surface waters (i.e. greater $\Delta\Delta^{14}C_{surf}$) are required; ~17 to 14.5 kyr BP and ~13 to 12 kyr BP. (C) Same as panel B except that the reference surface ocean $\Delta^{14}C$ curve was estimated using the ETD method (solid green line in panel A). Also shown is a time series of surface water reservoir age at 44°S in the Atlantic sector of the Southern Ocean (dashed line) (Skinner et al., 2010). (D) Opal flux records from south of the Antarctic Polar Front, including TN057-13-4PC (blue) and E27-23 (green) (Anderson et al., 2009). Calendar ages for each core (triangles) are based on the modern ΔR for the Southern Ocean south of 60°S (820±190 yr; CALIB Marine Database). The primary increase in opal flux at 16.0±0.5 kyr BP occurred ~1 kyr after the change in surface Southern Ocean $\Delta^{14}C$ implied by the deep Pacific data. An increase in surface water reservoir age of 800 yr would make the opal time series 1500 yr younger, amplifying the time lag between the opal records and $\Delta\Delta^{14}C$ estimates. (For interpretation of the references to color in this figure legend, the reader is referred to the web version of this article.)

$\Delta\Delta^{14}C$ time series appear to show broadly similar variability during the deglaciation.

An 800-yr increase in surface water reservoir age in the Southern Ocean would impact the age models for the opal records, causing both the reservoir-corrected radiocarbon ages and associated calendar ages to decrease. Core E27-23 has two calendar age control points near 16 kyr BP, including one at 15.9 kyr BP and another at 16.8 kyr BP (Fig. 7D). Each point was estimated assuming a modern ΔR of 800 yr (Anderson et al., 2009) and the INTCAL09 calibration curve (Reimer et al., 2009). If instead a ΔR of 1600 yr is applied (i.e. an 800-yr increase in reservoir age), the resulting calendar ages become 14.3 kyr BP and 15.4 kyr BP, ~1500 yr younger than the original values. In this scenario, the abrupt increase in opal flux during the deglaciation would occur at approximately 15 kyr BP, well after the implied increase in $\Delta\Delta^{14}C$ (which occurred by 17 kyr BP at the latest). The timing of the existing opal flux time series therefore does not support the hypothesis that upwelling influenced deep Pacific projection ages via changes in surface water reservoir age in the Southern Ocean. It is possible that additional upwelling proxies or estimates of surface water $\Delta^{14}C$ will suggest otherwise, but at present the evidence for such a driver is not compelling.

Given that the Southern Ocean is only one of the components that comprises water in the deep Northeast Pacific, it is important to consider possible changes in the other components listed in Table 1. The North Atlantic is an obvious candidate given its relatively young reservoir age (~400 yr) and paleoceanographic evidence for a reduction in the Atlantic meridional overturning circulation (AMOC) during both HS1 and the YD (McManus et al., 2004; Gherardi et al., 2009). Assuming a complete cessation of the AMOC, the net reservoir age of water entering the deep Pacific would increase to approximately 970 yr. Clearly this is too small to explain the ventilation age anomalies during the deglaciation. However, changing the AMOC would also indirectly influence the $\Delta^{14}C$ of other components used to estimate the net Pacific reservoir age. An increase in the net reservoir age of 800 yr can be achieved by removing the Atlantic component and increasing the Antarctic surface water age by 1000 yr.

Determining whether large surface ocean $\Delta^{14}C$ signals occurred during the deglaciation will require detailed modeling that characterizes the influence of ocean circulation variability on the $\Delta^{14}C$ tracer field as well as the influence of variable atmospheric $\Delta^{14}C$ on surface water reservoir ages. Results from an intermediate complexity model suggest that a 30% reduction in the AMOC superimposed on LGM boundary conditions increases the reservoir age in the southern ocean by several hundred years (Franke et al., 2008). Results from the same study indicate Southern Ocean reservoir ages can decrease by several hundred years during intervals of rapid atmospheric $\Delta^{14}C$ decline. Such an effect is apparent in the Fig. 7A where the ETD-based surface ocean $\Delta^{14}C$ curve suggests reservoir ages were lower during HS1 due to the large decrease in atmospheric $\Delta^{14}C$. Determining the interplay between AMOC and atmospheric $\Delta^{14}C$ variability should be a priority for future modeling studies. The $\Delta\Delta^{14}C$ estimates in Fig. 7 also point to a clear need for quantitative estimates of Southern Ocean reservoir age during the deglaciation.

3.5. Decreased ventilation of the deep Pacific

Given that neither the influence of mixing nor changes in source region reservoir age can easily explain the projection age results, it is important to consider the possibility that the benthic $\Delta^{14}C$ data reflect a real change in the ventilation rate of the deep Pacific. Rising surface temperatures during HS1 and the YD (Monnin et al., 2001) could conceivably increase water column stratification near Antarctica and limit ventilation. Unfortunately, a lack of vertical $\delta^{18}O$ profiles from the Southern Ocean precludes a detailed evaluation of this possibility. Greater stratification also runs counter to most hypotheses of the deglacial CO_2 rise which invoke vertical mixing to expose CO_2-rich deep waters to the atmosphere (e.g. Sigman et al., 2010). Opal flux results from south of the Antarctic Polar Front imply that deep upwelling and presumably westerly wind stress was enhanced during the deglaciation (Anderson et al., 2009).

The sensitivity of the meridional overturning circulation (MOC) to westerly windstress in the Southern Ocean is highly dependent on model resolution. Course resolution models generally show a strong positive MOC response to westerly windstress (Toggweiler and Samuels, 1995; Delworth and Zeng, 2008). Tschumi et al. (2011) found that an 80% increase in Southern Ocean wind stress causes the Atlantic MOC to more than double in magnitude and deep North Atlantic $\Delta^{14}C$ to increase by ~50‰. The modeled overturning response in the Pacific is more subdued, yielding an increase in $\Delta^{14}C$ below 2000 m of approximately 10‰. Farneti and Delworth (2010) found that increasing the zonal wind stress in a coarse resolution model (GFDL CM2.1) resulted in global MOC anomalies of 5–15 Sv at 40°S. In a finer resolution version of the same model (GFDL CM2.4) the primary circulation response was limited to the Southern Ocean and the global MOC anomaly at 40°S was 1–3 Sv. In this model the northward wind-driven Ekman transport is largely compensated by southward eddy fluxes, eliminating most of the global MOC signal observed in the coarser resolution simulation (Farneti and Delworth, 2010). Thus, even very large changes in Southern Hemisphere westerlies appear to have minimal impact on deep Pacific ventilation rate in eddy-resolving models. If such a change exists, it is towards younger ventilation ages, opposite the pattern observed during the deglaciation.

The results presented here suggest that the CO_2 increase during the deglaciation was not primarily driven by outgassing of carbon from the Pacific. On its own, reduced ventilation of the deep Pacific would tend to promote sequestration of respired carbon and draw down atmospheric CO_2. One alternative is a shift in the efficiency of the ocean's biological pump driven by variable deep water formation in the North Atlantic. In simulations where northern component water is shutdown via freshwater hosing, the ocean's preformed nutrient content and atmospheric CO_2 increase because the biological pump becomes less efficient at moving carbon from the surface into the deep ocean (Schmittner and Galbraith, 2008; Toggweiler et al., 2003). Although a full shutdown in northern component did not occur during HS1 (Gherardi et al., 2009), a change in nutrient utilization efficiency may be necessary to reconcile older deep Pacific ventilation ages and rising atmospheric CO_2 during the deglaciation.

4. Conclusions

The primary aim of this paper was to evaluate two key assumptions of the projection age method, including (1) that mixing plays a minor role in controlling $\Delta^{14}C$ in the ocean interior, and (2) that initial $\Delta^{14}C$ of waters entering the deep Pacific remains constant through time. The first point is addressed through the use of the TTD–ETD method, which takes into account the effect of advection and diffusion on $\Delta^{14}C$ (DeVries and Primeau, 2010). Data from the deep northeast and western equatorial Pacific are analyzed using the TTD–ETD method and each location yields a consistent history of Pacific ventilation during the deglaciation. Similar to the projection age results, the TTD–ETD approach yields a 1000-yr increase in ventilation age during HS1 and a 500-yr increase during the YD.

Centennial-scale offsets between the projection age and TTD–ETD results are primarily due to the different approaches used to estimate surface ocean radiocarbon content. Because the ETD tail extends thousands of years into the past, a given ETD-based

surface ocean $\Delta^{14}C$ estimate will reflect not only the contemporaneous atmospheric $\Delta^{14}C$ but also that of the preceding millennia. During intervals when atmospheric $\Delta^{14}C$ decreases, ETD-based $\Delta^{14}C$ estimates will be younger than those estimated assuming a constant reservoir age. The net effect is such that TTD ages are generally older than projection ages during the last 25 kyr. Using projection ages instead of transit time distributions introduces a small (<100 yr) bias in paleo-ventilation ages estimates, consistent with studies that evaluate the effect of TTD width on ventilation ages in the modern ocean (Gebbie and Huybers, 2012; Khatiwala et al., 2012).

One possible explanation of the ventilation age results is that the rate of the deep Pacific remained constant through time and the ventilation age anomalies were instead driven by changes in surface water reservoir age in the Southern Ocean. To test this idea, the deep Pacific $\Delta^{14}C$ data were un-decayed to estimate the reservoir ages necessary to explain the ventilation history. Surface water reservoir ages in the Southern Ocean would have to increase by 500–1000 yr and the timing of the changes is inconsistent with records of upwelling from the Southern Ocean. Although this mechanism cannot be ruled out at this stage, it appears to be an unlikely driver of the deep Pacific $\Delta^{14}C$ records.

It is also important to remember that the projection age and TTD approaches as applied here are overly simplistic in that they assume the initial age of water entering the deep Pacific is set largely in the Southern Ocean. If this was not the case during the deglaciation then the assumptions used here regarding surface water reservoir ages and ETDs would need to be re-evaluated. Removing the young North Atlantic contribution to the net surface water reservoir age for the deep Pacific has only a modest impact. However, the total downstream effect of such a perturbation on the $\Delta^{14}C$ in other regions that contribute to the deep Pacific will require more comprehensive modeling. Formation of a new deep watermass in the North Pacific would tend to increase the $\Delta^{14}C$ content of deep waters, opposite the pattern observed. Carbon from a geological source (e.g. Stott and Timmermann, 2011; Lund and Asimow, 2011) could potentially explain ^{14}C deficits during the deglaciation but these mechanisms must first be verified using data that more directly reflect such inputs.

Prevailing hypotheses regarding the rise of atmospheric CO_2 during the deglaciation center around the Southern Ocean, generally calling for enhanced upwelling of CO_2-rich deep water linked to intensification of the Southern Hemisphere westerlies (Anderson et al., 2009; Sigman et al., 2010). Although the sensitivity of the global meridional overturning to westerly winds is highly dependent on model resolution, both eddy and non-eddy resolving models suggest that ventilation ages in the deep Pacific should have decreased during the deglaciation rather than increased. Resolving this fundamental discrepancy will be key to understanding the ocean's role in glacial–interglacial CO_2 cycles.

Acknowledgements

I would like to thank Tim DeVries for providing the TTD–ETD Matlab code and patiently responding to questions about the code and the TTD–ETD method in general. I would also like to thank Eric Galbraith, John Southon, Wally Broecker, and Laura Robinson for insightful discussions. This work was supported by the University of Michigan.

References

Adkins, J.F., Boyle, E.A., 1997. Changing atmospheric Delta C-14 and the record of deep water paleoventilation ages. Paleoceanography 12, 337–344.

Anderson, R.F., Ali, S., Bradtmiller, L.I., Nielsen, S.H.H., Fleisher, M.Q., Anderson, B.E., Burckle, L.H., 2009. Wind-driven upwelling in the Southern Ocean and the deglacial rise in atmospheric CO_2. Science 323, 1443–1448.

Broecker, W., Clark, E., Barker, S., 2008. Near constancy of the Pacific Ocean surface to mid-depth radiocarbon-age difference over the last 20 kyr. Earth Planet. Sci. Lett. 274, 322–326.

Clark, P.U., Dyke, A.S., Shakun, J.D., Carlson, A.E., Clark, J., Wohlfarth, B., Mitrovica, J.X., Hostetler, S.W., McCabe, A.M., 2009. The last glacial maximum. Science 325, 710–714.

Curry, W.B., Oppo, D.W., 2005. Glacial water mass geometry and the distribution of delta C-13 of Sigma CO2 in the western Atlantic Ocean. Paleoceanography 20.

Delworth, T.L., Zeng, F.R., 2008. Simulated impact of altered Southern Hemisphere winds on the Atlantic Meridional Overturning Circulation. Geophys. Res. Lett. 35, 5.

DeVries, T., Primeau, F., 2010. An improved method for estimating water-mass ventilation age from radiocarbon data. Earth Planet. Sci. Lett. 295, 367–378.

Farneti, R., Delworth, T.L., 2010. The role of mesoscale eddies in the remote oceanic response to altered southern hemisphere winds. J. Phys. Oceanogr. 40, 2348–2354.

Franke, J., Paul, A., Schulz, M., 2008. Modeling variations of marine reservoir ages during the last 45,000 years. Clim. Past 4, 125–136.

Galbraith, E.D., Jaccard, S.L., Pedersen, T.F., Sigman, D.M., Haug, G.H., Cook, M., Southon, J.R., Francois, R., 2007. Carbon dioxide release from the North Pacific abyss during the last deglaciation. Nature 449, 890–899.

Gebbie, G., Huybers, P., 2010. Total matrix intercomparison: A method for determining the geometry of water-mass pathways. J. Phys. Oceanogr. 40, 1710–1728.

Gebbie, G., Huybers, P., 2012. The mean age of ocean waters inferred from radiocarbon observations: Sensitivity to surface sources and accounting for mixing histories. J. Phys. Oceanogr. 42, 291–305.

Gebhardt, H., Sarnthein, M., Grootes, P.M., Kiefer, T., Kuehn, H., Schmieder, F., Rohl, U., 2008. Paleonutrient and productivity records from the subarctic North Pacific for Pleistocene glacial terminations I to V. Paleoceanography 23, 21.

Gherardi, J.M., Labeyrie, L., Nave, S., Francois, R., McManus, J.F., Cortijo, E., 2009. Glacial–interglacial circulation changes inferred from Pa-231/Th-230 sedimentary record in the North Atlantic region. Paleoceanography 24, 14.

Herguera, J.C., Herbert, T., Kashgarian, M., Charles, C., 2010. Intermediate and deep water mass distribution in the Pacific during the Last Glacial Maximum inferred from oxygen and carbon stable isotopes. Quat. Sci. Rev. 29, 1228–1245.

Hoffman, J.L., Lund, D.C., 2012. Refining the stable isotope budget for Antarctic Bottom Water: New foraminiferal data from the abyssal Southwest Atlantic. Paleoceanography 27, PA1213, http://dx.doi.org/10.1029/2011PA002216.

Kawabe, M., Fujio, S., 2010. Pacific ocean circulation based on observation. J. Oceanogr. 66, 389–403.

Key, R.M., Kozyr, A., Sabine, C.L., Lee, K., Wanninkhof, R., Bullister, J.L., Feely, R.A., Millero, F.J., Mordy, C., Peng, T.H., 2004. A global ocean carbon climatology: Results from Global Data Analysis Project (GLODAP). Glob. Biogeochem. Cycles 18, 23.

Khatiwala, S., Primeau, F., Holzer, M., 2012. Ventilation of the deep ocean constrained with tracer observations and implications for radiocarbon estimates of ideal mean age. Earth Planet. Sci. Lett. 325–326, 116–125.

Lovenduski, N.S., Gruber, N., Doney, S.C., Lima, I.D., 2007. Enhanced CO2 outgassing in the Southern Ocean from a positive phase of the Southern Annular Mode. Glob. Biogeochem. Cycles 21, 14.

Lund, D.C., Asimow, P.D., 2011. Does sea level influence mid-ocean ridge magmatism on Milankovitch timescales? Geochem. Geophys. Geosyst. 12, http://dx.doi.org/10.1029/2011GC003693.

Lund, D.C., Mix, A.C., Southon, J., 2011. Increased ventilation age of the deep northeast Pacific Ocean during the last deglaciation. Nat. Geosci., http://dx.doi.org/10.1038/ngeo1272.

Lynch-Stieglitz, J., Adkins, J.F., Curry, W.B., Dokken, T., Hall, I.R., Herguera, J.C., Hirschi, J.J.M., Ivanova, E.V., Kissel, C., Marchal, O., Marchitto, T.M., McCave, I.N., McManus, J.F., Mulitza, S., Ninnemann, U., Peeters, F., Yu, E.F., Zahn, R., 2007. Atlantic meridional overturning circulation during the Last Glacial Maximum. Science 316, 66–69.

Mantyla, A.W., 1975. Potential temperature in Abyssal Pacific Ocean. J. Mar. Res. 33, 341–354.

Marshall, J., Speer, K., 2012. Closure of the meridional overturning circulation through Southern Ocean upwelling. Nat. Geosci. 5, 171–180.

McManus, J.F., Francois, R., Gherardi, J.M., Keigwin, L.D., Brown-Leger, S., 2004. Collapse and rapid resumption of Atlantic meridional circulation linked to deglacial climate changes. Nature 428, 834–837.

Monnin, E., Indermuhle, A., Dallenbach, A., Fluckiger, J., Stauffer, B., Stocker, T.F., Raynaud, D., Barnola, J.M., 2001. Atmospheric CO_2 concentrations over the last glacial termination. Science 291, 112–114.

Monnin, E., Steig, E.J., Siegenthaler, U., Kawamura, K., Schwander, J., Stauffer, B., Stocker, T.F., Morse, D.L., Barnola, J.M., Bellier, B., Raynaud, D., Fischer, H., 2004. Evidence for substantial accumulation rate variability in Antarctica during the Holocene, through synchronization of CO_2 in the Taylor Dome, Dome C and DML ice cores. Earth Planet. Sci. Lett. 224, 45–54.

Rasmussen, S.O., Andersen, K.K., Svensson, A.M., Steffensen, J.P., Vinther, B.M., Clausen, H.B., Siggard-Andersen, M.L., Johnsen, S.J., Larsen, L.B., Dahl-Jensen, D., Bigler, M., Rothlisberger, R., Fischer, H., Goto-Azuma, K., Hansson, M.E., Ruth, U., 2006. A new Greenland ice core chronology for the last glacial termination. J. Geophys. Res. 111.

Reimer, P.J., Baillie, M.G.L., Bard, E., Bayliss, A., Beck, J.W., Blackwell, P.G., Ramsey, C.B., Buck, C.E., Burr, G.S., Edwards, R.L., Friedrich, M., Grootes, P.M., Guilderson, T.P., Hajdas, I., Heaton, T.J., Hogg, A.G., Hughen, K.A., Kaiser, K.F., Kromer, B., McCormac, F.G., Manning, S.W., Reimer, R.W., Richards, D.A., Southon, J.R., Talamo, S., Turney, C.S.M., van der Plicht, J., Weyhenmeye, C.E., 2009. INTCAL09 and MARINE09 radiocarbon age calibration curves, 0–50,000 years CAL BP. Radiocarbon 51, 1111–1150.

Schmitt, J., et al., 2012. Carbon isotopic constraints on the deglacial CO_2 rise from ice cores. Science 336, http://dx.doi.org/10.1126/science.1217161.

Schmittner, A., Galbraith, E.D., 2008. Glacial greenhouse-gas fluctuations controlled by ocean circulation changes. Nature 456, 373–376.

Shakun, J.D., Clark, P.U., He, F., Marcott, S.A., Mix, A.C., Liu, Z.Y., Otto-Bliesner, B., Schmittner, A., Bard, E., 2012. Global warming preceded by increasing carbon dioxide concentrations during the last deglaciation. Nature 484.

Sigman, D.M., Boyle, E.A., 2000. Glacial/interglacial variations in atmospheric carbon dioxide. Nature 407, 859–869.

Sigman, D.M., Hain, M.P., Haug, G.H., 2010. The polar ocean and glacial cycles in atmospheric CO_2 concentration. Nature 466, 47–55.

Skinner, L.C., Fallon, S., Waelbroeck, C., Michel, E., Barker, S., 2010. Ventilation of the Deep Southern Ocean and deglacial CO_2 rise. Science 328, 1147–1151.

Stott, L.D., Timmermann, A., 2011. Hypothesized link between glacial/interglacial CO_2 cycles and storage/release of CO_2-rich fluids from the deep sea. In: Understanding the Causes, Mechanisms, and Extent of the Abrupt Climate Change. In: Geophys. Monogr. Ser., vol. 193. American Geophysical Union.

Toggweiler, J.R., Murnane, R., Carson, S., Gnanadesikan, A., Sarmiento, J.L., 2003. Representation of the carbon cycle in box models and GCMs – 2. Organic pump. Glob. Biogeochem. Cycles 17, 13.

Toggweiler, J.R., Samuels, B., 1995. Effect of drake passage on the global thermohaline circulation. Deep-Sea Res., Part 1, Oceanogr. Res. Pap. 42, 477–500.

Tschumi, T., Joos, F., Gehlen, M., Heinze, C., 2011. Deep ocean ventilation, carbon isotopes, marine sedimentation and the deglacial CO_2 rise. Clim. Past 7, 771–800.